

Dendritic Compartment and Neuronal Output Mode Determine Pathway-Specific Long-Term Potentiation in the Piriform Cortex

Friedrich W. Jochenning,¹ Prateep S. Beed,¹ Thorsten Trimbuch,² Michael H. K. Bendels,^{1,3} Jochen Winterer,¹ and Dietmar Schmitz^{1,4}

¹Neuroscience Research Center, ²Institute for Cell Biology and Neurobiology, Center for Anatomy, and ³Neurophysics Group, Department of Neurology, Charité-Universitätsmedizin Berlin, 10117 Berlin, Germany, and ⁴Bernstein Center for Computational Neuroscience Berlin, 10115 Berlin, Germany

The apical dendrite of layer 2/3 pyramidal cells in the piriform cortex receives two spatially distinct inputs: one projecting onto the distal apical dendrite in sensory layer 1a, the other targeting the proximal apical dendrite in layer 1b. We observe an expression gradient of A-type K⁺ channels that weakens the backpropagating action potential-mediated depolarization in layer 1a compared with layer 1b. We find that the pairing of presynaptic and postsynaptic firing leads to significantly smaller Ca²⁺ signals in the distal dendritic spines in layer 1a compared with the proximal spines in layer 1b. The consequence is a selective failure to induce long-term potentiation (LTP) in layer 1a, which can be rescued by pharmacological enhancement of action potential backpropagation. In contrast, LTP induction by pairing presynaptic and postsynaptic firing is possible in layer 1b but requires bursting of the postsynaptic cell. This output mode strongly depends on the balance of excitation and inhibition in the piriform cortex. We show, on the single-spine level, how the plasticity of functionally distinct synapses is gated by the intrinsic electrical properties of piriform cortex layer 2 pyramidal cell dendrites and the cellular output mode.

Introduction

Two spatially distinct pathways project onto the apical dendrites of layer 2/3 pyramidal cells in layer 1 of the piriform cortex. Direct synaptic inputs from mitral cells in the olfactory bulb project onto the distal portion of the dendrite, constituting the sensory layer 1a. Associational synapses from within the piriform cortex and other brain areas cluster in the proximal layer 1b (Neville and Haberly, 2004). This laminar structure allows a clear spatial distinction between sensory and associative inputs. A key functional difference between the two synaptic inputs is their plasticity. NMDA receptor (NMDAR)-dependent long-term potentiation (LTP) of synaptic contacts is much more pronounced in the proximal associative layer 1b than in the distal sensory layer 1a (Jung et al., 1990a,b; Kanter and Haberly, 1990; Franks and Isaacson, 2005; Poo and Isaacson, 2007). So far, mechanisms determining the weakness of layer 1a LTP have only been found on the level of LTP expression (Franks and Isaacson, 2005). The induction of LTP by pairing EPSPs with subsequent action potentials

(APs) is reduced in the distal dendrites in neocortical pyramidal cells and in the CA1 pyramidal cells in the hippocampus. In these neurons, the attenuated distal propagation of backpropagating APs (bAPs), mediated by the intrinsic electrical properties of the dendritic tree, weakens distal LTP induction (Golding et al., 2002; Letzkus et al., 2006; Sjöström and Häusser, 2006).

In area CA1 within the hippocampal formation and also the neocortex, LTP can be induced by pairing EPSPs with bursts of APs (Pike et al., 1999; Kampa et al., 2006; Letzkus et al., 2006; Nevian and Sakmann, 2006). It has been demonstrated by Suzuki and Bekkers that intrinsic AP bursting during suprathreshold depolarization is a key feature of piriform cortex pyramidal cells. In the same study, short bursts with high instantaneous firing frequencies of up to 150 Hz were evoked by strong stimulation of sensory or associative pathways with typical sensory input patterns (Suzuki and Bekkers, 2006). During sniffing, short AP bursts with instantaneous firing rates above 100 Hz have also been observed in intracellular recordings *in vivo* (Wilson, 1998). Recently, it has been shown *in vitro* that selective stimulation of the sensory lateral olfactory tract (LOT) input to layer 1a results in prominent feedforward inhibition, limiting the output mode to single action potentials. A reduction in inhibitory drive turned these single APs into short bursts (Luna and Schoppa, 2008). Bursting and single-spike firing modes of pyramidal cells in the piriform cortex appear tightly controlled by the ratio of excitation (synaptic and intrinsic) to inhibition.

During LTP induction, Ca²⁺ signals in postsynaptic spines are a key determinant of plasticity outcome (Nevian and Sakmann, 2006) (for review, see Sjöström et al., 2008). Here, we analyze Ca²⁺ sig-

Received June 8, 2009; revised July 24, 2009; accepted Aug. 5, 2009.

This work was supported by Deutsche Forschungsgemeinschaft Grants EXC 257, GRK 1123, SFB 618, and SFB 665 and the Bundesministerium für Bildung und Forschung (Bernstein Center for Computational Neuroscience Berlin). P.S.B. is a member of GRK 1123 (Berlin, Germany). We thank Genela Morris, Jörg Breustedt, Knut Holthoff, and Sarah Shoichet for critically reading this manuscript and Susanne Walden, Anke Schönherr, and Denis Lajkó for excellent technical assistance.

Correspondence should be addressed to either Dietmar Schmitz or Friedrich W. Jochenning, Neurowissenschaftliches Forschungszentrum, Charité-Universitätsmedizin Berlin, Charitéplatz 1, 10117 Berlin, Germany. E-mail: dietmar.schmitz@charite.de or friedrich.jochenning@charite.de.

DOI:10.1523/JNEUROSCI.2672-09.2009

Copyright © 2009 Society for Neuroscience 0270-6474/09/2913649-13\$15.00/0

nals in proximal and distal dendritic segments within pyramidal neurons of the piriform cortex. We demonstrate that the laminar distribution of different synaptic inputs is a prerequisite for differences in synaptic plasticity induction based on the electrical compartmentalization of the dendritic tree. We further propose that LTP induction in the plasticity-competent layer 1b synapses is gated by the neuronal output mode (single APs vs bursting).

Materials and Methods

Electrophysiology

Preparation. Coronal slices of the anterior piriform cortex were prepared from Wistar rats [aged postnatal day 19 (P19) to P25]. All procedures were performed in accordance with national and international guidelines. Animals were anesthetized and decapitated. The brains were quickly removed into ice-cold artificial CSF (ACSF) containing the following (in mM): 87 NaCl, 26 NaHCO₃, 25 glucose, 2.5 KCl, 7 MgCl₂, 1.25 NaH₂PO₄, 0.5 CaCl₂, and 75 sucrose, pH 7.4. Tissue blocks were mounted on a vibratome (VT 1200; Leica Microsystems), cut at 300 μ m thickness, and incubated at 35°C for 30 min. The slices were then transferred to ACSF containing the following (in mM): 119 NaCl, 26 NaHCO₃, 10 glucose, 2.5 KCl, 2.5 CaCl₂, 1 MgSO₄, and 1 NaH₂PO₄. For LTP experiments, 2 μ M gabazine was added. For the 4-AP experiments looking at bAP-mediated Ca²⁺, 25 μ M NBQX, 50 μ M D-APV, and 2 μ M gabazine were added to the ACSF. LTP experiments in the presence of 4-AP were performed in 2 μ M gabazine and 100 nM NBQX. The slices were stored at room temperature in a submerged chamber for 1–5 h before being transferred to the recording chamber.

Whole-cell recordings. Whole-cell voltage-clamp and current-clamp recordings were performed with an Axopatch 700B Amplifier (Molecular Devices) at 28–30°C. Data were digitized at 5 kHz and low-pass filtered at 2 kHz. For Ca²⁺ imaging experiments, patch electrodes [electrode resistances ranging from 3 to 6 M Ω were filled with the following (in mM): 115 K-gluconate, 20 KCl, 10 HEPES, 4 MgATP, 0.3 Na-GTP, and 10 phosphocreatine, pH 7.3 with KOH]. Oregon-Green BAPTA-1 (OGB1) was added at 100 μ M and Oregon-Green BAPTA-6F (OGB6F) at 200 μ M. For LTP experiments, the intracellular solution consisted of the following (in mM): 130 K-gluconate, 20 KCl, 10 HEPES, 4 MgATP, 0.3 Na-GTP, and 10 phosphocreatine, pH 7.4 with KOH. Initial access resistances were in the range of 10 and 20 M Ω after breakthrough and not allowed to vary >20% during the course of the experiment in the voltage-clamp mode. No access resistance compensation was used.

APs were induced with 2 ms pulses at 1–3 nA. Synaptic stimulation was performed with patch pipettes filled with ACSF. For LTP measurements, the pipette was placed at the layer 2–layer 1b border for layer 1b stimulation and at the LOT–layer 1a border for layer 1a stimulation (see Fig. 6A). The test stimulus was applied in the voltage-clamp mode, the amplitude was between 50 and 200 pA. For LTP induction, the amplifier was switched to current clamp. Stimulus artifacts are clipped in all figures.

Morphological reconstruction

Slices with biocytin-filled cells were fixed in 0.1 M phosphate buffer, pH 7.4, containing 4% paraformaldehyde (PFA), for 24–48 h. The filled neurons were visualized by incubating sections in avidin–biotin-conjugated horseradish peroxidase (ABC; Vector Laboratories) and reacting them with diaminobenzidine and hydrogen peroxide. Sections were then dehydrated and embedded on glass slides. Subsequently, the cells were reconstructed with the aid of a NeuroLucida 3D reconstruction system (MicroBrightField).

Immunohistochemistry

For immunohistochemistry, P21 rats were anesthetized (0.5% ketamine, i.p.) and transcardially perfused with 4% PFA. Brains were postfixed overnight in 4% PFA and cut on a vibratome. Sections at 50 μ m were blocked for 1 h (5% normal goat serum and 0.1% Triton X-100) before overnight incubation with antibodies against rabbit Kv4.2/4.3 (H-225) (1:200; Santa Cruz Biotechnology) and mouse MAP2 (HM-2) (1:1000; Sigma). Sections were immunostained with Alexa-labeled secondary antibodies (Invitrogen). Images were obtained with a Leica Microsystems

confocal laser-scanning microscope (TCS SL). For quantification of Kv4.2/4.3 expression in the piriform cortex layers 1a and 1b, randomly chosen 50 \times 50 μ m subregions aligned to follow the main vertical dendritic axis were scanned with a 63 \times oil objective (zoom 5, same configurations in both areas) and quantified using MetaMorph (version 6.2r6). The number of Kv4.2/4.3 puncta was related to the MAP2 contour distance as an indicator of dendritic segment density. To avoid bias, all quantifications were performed using the same predefined journals (Mokin and Keifer, 2006). Kv4.2/4.3 puncta were defined as an area >5 pixels (0.01 μ m²) to exclude unspecific background signals.

Ca²⁺ imaging

For time-lapse confocal recordings, a Yokogawa CSU-22 spinning disc confocal system (BFi OPTiLAS) was used with an Olympus BX-51WI upright microscope and a RedShirt NeuroCCD-SMQ camera (Life Imaging Services). Excitation was provided at 488 nm by a Coherent Sapphire 488-50 Laser (Coherent). Using the Olympus LumPlan FI 60 \times , 0.9 numerical aperture water-immersion objective, the power under the objective was typically 5–20 μ W. When using the same objective, the lateral pixel size was 0.4 μ m, and the pinhole size of the Yokogawa CSU-22 spinning disc confocal corresponded to 1.18 Airy units at 520 nm emission wavelength. Full frames were recorded at 125 Hz. Imaging was started 20–30 min after breakthrough. For spine stimulation, the stimulation pipette was placed within 10–30 μ m of the imaged spine. When searching for spines, there is a bias against small spines and synapses with a very low *p*. Silent synapses will not be detected with synaptic stimulation at –75 mV holding potential. Spines were only used for experiments when stable responses could be elicited from well isolated Ca²⁺ sources (see Fig. 4A). Experiments were discarded if there was a change in absolute baseline brightness >20% or increase in τ >20%.

Analysis

All imaging data displayed (unless otherwise noted) and used for quantitative analysis are averages of three to five sweeps. When synaptically stimulating single spines for Ca²⁺ imaging, synaptic failures were not included in the averages to exclude presynaptic effects. The criterion for defining transmission failures and successes as well as significant back-propagating AP responses was a peak amplitude two times larger than the SD of the baseline noise. See Figure 4A for distinction between successes and failures on the single-trial level. The signal amplitudes were obtained from exponential fits of averaged traces starting at signal initiation. Ratios were formed as pairwise comparisons in individual cells.

For LTP measurements, only experiments were included that displayed stable recording conditions for longer than 15 min after LTP induction. LTP was quantified for statistical comparisons by normalizing and averaging EPSC amplitudes between 20 and 25 min after induction to 4 min of baseline. In the 4-AP LTP experiments, the analysis was performed on a time interval 15–20 min after induction. Displayed traces are averages of the sweeps corresponding to this time interval.

All data are displayed as means \pm SEM. To determine statistical significances, we used two-tailed unpaired Student's *t* tests or paired *t* tests as appropriate, a Mann–Whitney *U* test in which data was not normally distributed (Shapiro–Wilk test), or a one-way ANOVA, followed by Tukey's multiple comparison test. Differences were called significant if *p* < 0.05.

Results

Attenuation of the bAP-mediated dendritic Ca²⁺ signal in the sensory layer 1a

Pyramidal cells in layer 2 of the anterior piriform cortex were identified by their typical morphology and intrinsic electrical properties (an initial burst fired after suprathreshold somatic current injection; shown in Fig. 1A) (Suzuki and Bekkers, 2006). A spinning disc confocal with a fast CCD camera was used for Ca²⁺ imaging. Neurons were loaded with the high-affinity Ca²⁺ indicator OGB1 or the medium-affinity Ca²⁺ indicator OGB6F for 25 min via the patch pipette before recording. Somatic APs were evoked by suprathreshold current injection (1–3 nA for 2

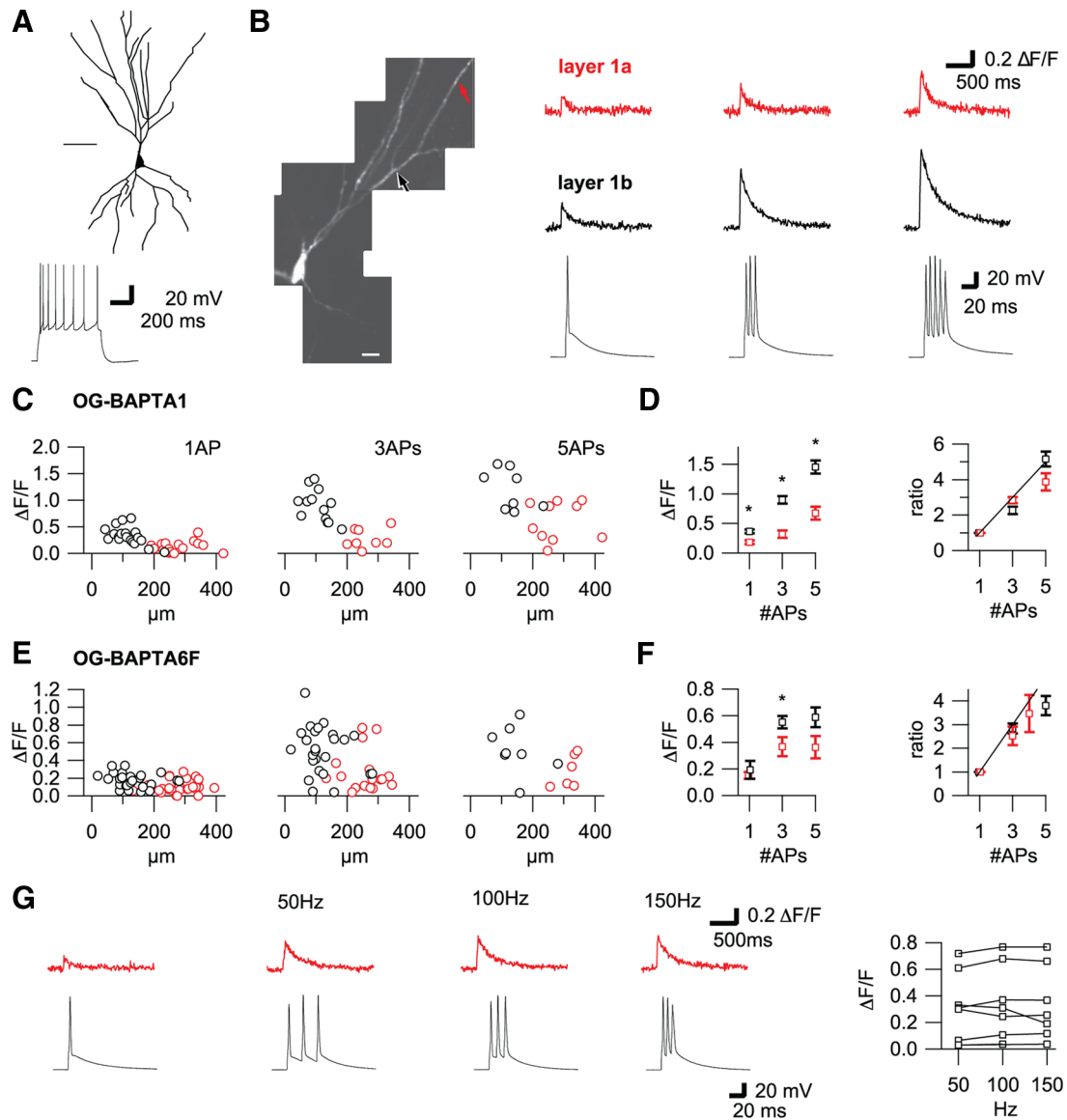


Figure 1. Properties of backpropagating AP-mediated dendritic Ca^{2+} signals in layer 1a and 1b. **A**, Top, Camera lucida reconstruction of a biocytin-filled layer II pyramidal cell in the anterior piriform cortex. Scale bar, 50 μm . Bottom, Firing pattern evoked by suprathreshold somatic current injection. **B**, Left, Montage of a layer 2 pyramidal cell in the anterior piriform cortex filled with OGB6F. Arrows point at dendritic regions corresponding to Ca^{2+} traces on the right. Right, Ca^{2+} signals in layer 1a (top) and layer 1b (middle) evoked by one, three, and five APs at 150 Hz (bottom). **C**, Scatter plot of peak Ca^{2+} measured with OGB1 versus distance from the soma for one, three, and five APs. **D**, Left, Averaged peak amplitudes of significant responses are larger in layer 1b than in layer 1a at one ($n = 17$ and 9, respectively), three ($n = 13$ and 7, respectively), and five ($n = 10$ and 9, respectively; $p < 0.01$) APs. Right, Ratios of three (layer 1b, $n = 12$; layer 1a, $n = 5$) and five (layer 1b, $n = 9$; layer 1a, $n = 6$) APs over one AP display sublinear to linear addition of APs in layer 1a and layer 1b. **E**, Scatter plot of peak Ca^{2+} measured with OGB6F versus distance from the soma for one, three, and five APs. **F**, Left, Averaged peak amplitudes of significant responses are larger in layer 1b than in layer 1a at one ($n = 23$ and 9, respectively; $p > 0.1$), three ($n = 24$ and 11, respectively; $p < 0.05$), and five ($n = 7$ and 4, respectively; $p > 0.05$) APs. Right, Ratios of three (layer 1b, $n = 18$; layer 1a, $n = 8$) and five (layer 1b, $n = 7$) or four (layer 1a, $n = 3$) APs over one AP display sublinear to linear addition of APs in layer 1a and layer 1b. **G**, Left, Time course of Ca^{2+} signals in layer 1a (top) evoked by one AP and three APs at 50, 100, and 150 Hz (bottom). Right, Plot of peak amplitudes of Ca^{2+} signals at 50, 100, and 150 Hz.

ms). bAP-mediated Ca^{2+} responses were measured in different regions of the dendritic tree. The distance of the imaged dendritic region from the soma was measured using a *post hoc* reconstruction of the dye-filled cell (Fig. 1B). On small magnification differential interference contrast (DIC) images, layer 1a and layer 1b could be distinguished by their different brightness (see Fig. 6A). In addition to the absolute distance, the synaptic layer was attributed to each imaging site by localizing corresponding image points on the DIC and the CCD image.

When using the high-affinity Ca^{2+} indicator OGB1, Ca^{2+} responses to single bAPs could be detected throughout the dendritic tree. There was a clear decrease in the amplitude of the

bAP-evoked Ca^{2+} response with distance from the soma (Fig. 1C); the average amplitude of significant single bAP responses was $0.36 \pm 0.03 \Delta F/F$ ($n = 17$) in layer 1b and $0.18 \pm 0.03 \Delta F/F$ ($n = 9$) in layer 1a ($p < 0.01$).

No regenerative Ca^{2+} responses to high-frequency bursts in distal dendrites

In the apical dendrites of layer 2/3 and layer 5 neocortical pyramidal cells and in basal dendrites of layer 5 cells, the distance-dependent attenuation of the bAP-evoked Ca^{2+} response can be bypassed: short bursts of APs in the range of up to 150 Hz evoke regenerative supralinear dendritic Ca^{2+} responses in distal den-

drites (Larkum et al., 1999a; Waters et al., 2003; Kampa and Stuart, 2006; Larkum et al., 2007). Applying comparable somatic high-frequency bursts, similar behavior of layer 2 pyramidal cells of the piriform cortex could not be confirmed. Based on observations from previous *in vitro* and *in vivo* experiments (Wilson, 1998; Suzuki and Bekkers, 2006), we tested bursts of three and five APs at 150 Hz. For three APs, the average Ca^{2+} signal amplitude, as measured with OGB1, was $0.9 \pm 0.08 \Delta F/F$ in layer 1b ($n = 13$) and $0.32 \pm 0.06 \Delta F/F$ in layer 1a ($n = 7$; $p < 0.01$). The ratio of the Ca^{2+} response for three bAPs to that for one bAP was determined in individual cells. For layer 1a and 1b, ratio values were comparable (2.84 ± 0.18 , $n = 12$ for layer 1b and 2.26 ± 0.41 , $n = 5$ for layer 1a). Similar results were obtained with five AP bursts (Fig. 1D), suggesting that, at high $[\text{Ca}^{2+}]$, the high-affinity Ca^{2+} indicator OGB1 might be saturated. For this reason, the experiments were repeated with the medium-affinity Ca^{2+} indicator OGB6F (Fig. 1E). In comparing effects of three bAPs and one bAP, the ratios of significant Ca^{2+} responses were 2.84 ± 0.21 ($n = 18$) for layer 1b and 2.52 ± 0.39 ($n = 8$) for layer 1a (Fig. 1F). This lack of supralinearity was also confirmed for the relationship between values associated with five and one bAPs in layer 1b and four and one bAPs in layer 1a. The observed absence of supralinearity in distal dendrites was consistent over a broad range of frequencies, again using the medium-affinity Ca^{2+} indicator OGB6F (Fig. 1G). The ratio of significant Ca^{2+} transients evoked by bursts of three APs at 150 Hz to that at 100 Hz was 1.00 ± 0.08 ($n = 5$), and the ratio for values at 150 Hz to those at 50 Hz was 1.19 ± 0.19 ($n = 5$).

Synapse-specific dendritic compartmentalization mediated by A-type K^+ conductances

The differential distribution of intrinsic conductances in layer 1a and layer 1b could explain the observed attenuation of Ca^{2+} transients during bAP-induced voltage changes. For this reason, we examined the immunohistochemical distribution of Kv4.2 and Kv4.3, the two main subtypes constituting the dendritic A-type K^+ current (for review, see Birnbaum et al., 2004). Figure 2A shows the higher expression levels of Kv4.2 and Kv4.3 in the distal dendrites. As seen at a high magnification, the surface expression of the K^+ channel subunits in relation to the cytosolic MAP2 stain is higher in layer 1a than in layer 1b. The results are representative of five independently processed animals. As a result of neuronal branching, it is conceivable that the higher distal expression is based on a higher density of thinner dendritic branches in layer 1a. To address this question, we quantified the data morphometrically,

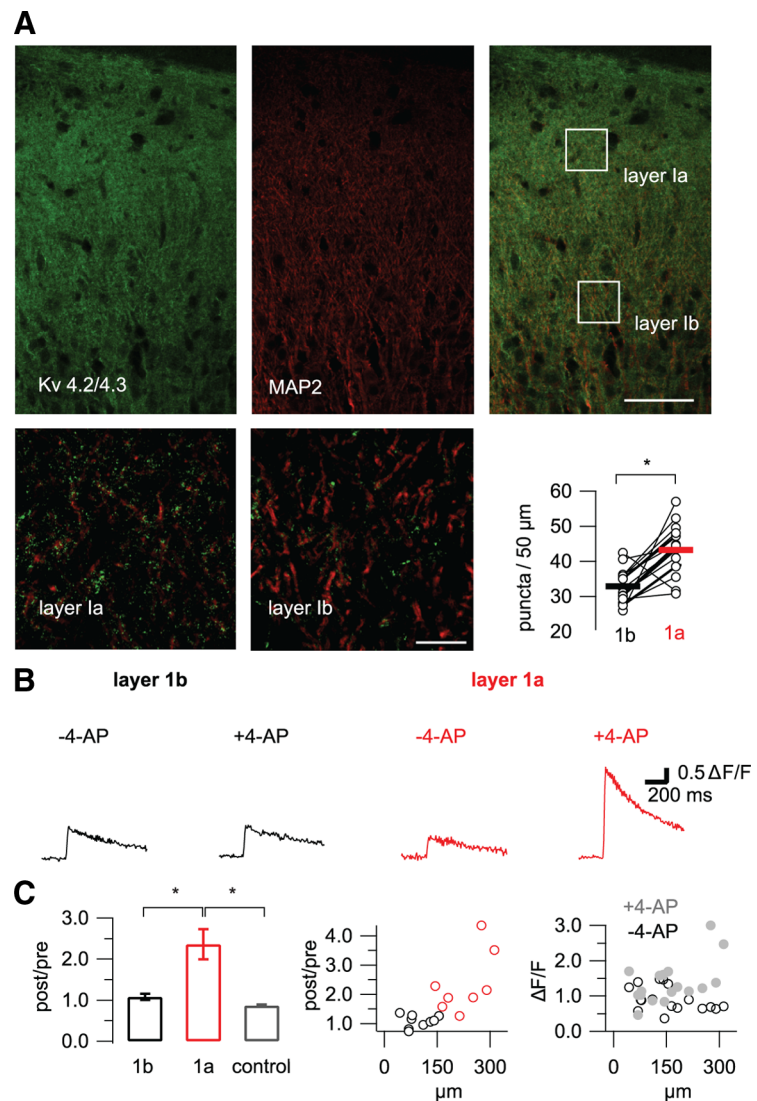


Figure 2. A distance-dependent increase in A-type K^+ conductances results in attenuation of distal Ca^{2+} signals in dendrites. **A**, Immunohistochemistry using MAP2- and Kv4.2/4.3-specific antibodies revealed different expression levels of A-type K^+ channels within the apical dendrites of the pyramidal cell. Top, Overview of the anterior piriform cortex demonstrating higher expression of Kv4.2/4.3 in distal dendrites corresponding to layer 1a. Scale bar, 100 μm . Bottom, High-magnification MAP2 and Kv4.2/4.3 stainings corresponding to the insets in the top merged picture from layer 1a and layer 1b demonstrate the higher surface expression levels of Kv4.2/4.3 in layer 1a. Scale bar, 10 μm . Bottom right, Plot of the number of Kv4.2/4.3-positive puncta per 50 μm of dendritic length in corresponding layer 1a and layer 1b segments. The Kv4.2/4.3 density is significantly higher in layer 1a ($n = 15$ slices from 5 animals; $p < 0.01$). **B**, Time courses of dendritic Ca^{2+} signals evoked by three APs at 150 Hz and measured with OGB1 from two different cells in layer 1b (left) and layer 1a (right). Fifteen minutes of wash-in of 4-AP increases the Ca^{2+} signal only in layer 1a. **C**, Left, 4-AP increases the Ca^{2+} signals evoked by three APs at 150 Hz in layer 1a ($n = 9$) but not in layer 1b ($n = 8$; $*p < 0.01$) and controls ($n = 5$; $*p < 0.01$). Middle, Plot of the ratio of peak Ca^{2+} signals post-4-AP over pre-4-AP application versus distance. The post/pre ratio increases with distance from the soma. Right, Plot of peak Ca^{2+} signals in 4-AP versus distance does not display the distance-dependent attenuation observed in control conditions.

normalizing the number of green puncta in layer 1a and layer 1b to the dendritic length (see Materials and Methods). In layer 1b, we counted an average of 33.1 ± 1.2 Kv4.2/4.3 puncta per 50 μm dendritic length. In the corresponding layer 1a segments, the Kv4.2/4.3 expression density was significantly increased to 43.4 ± 1.9 puncta per 50 μm dendritic length. This resulted in a layer 1a to 1b expression ratio of 1.34 ± 0.08 ($n = 15$ slices from 5 animals; $p < 0.01$). To validate this result, we subsequently examined the effect of the A-type K^+ channel blocker 4-AP. Application of 4 mM 4-AP resulted in a 2.4 ± 0.37 -fold increase in the amplitude of the Ca^{2+} response evoked by three bAPs com-

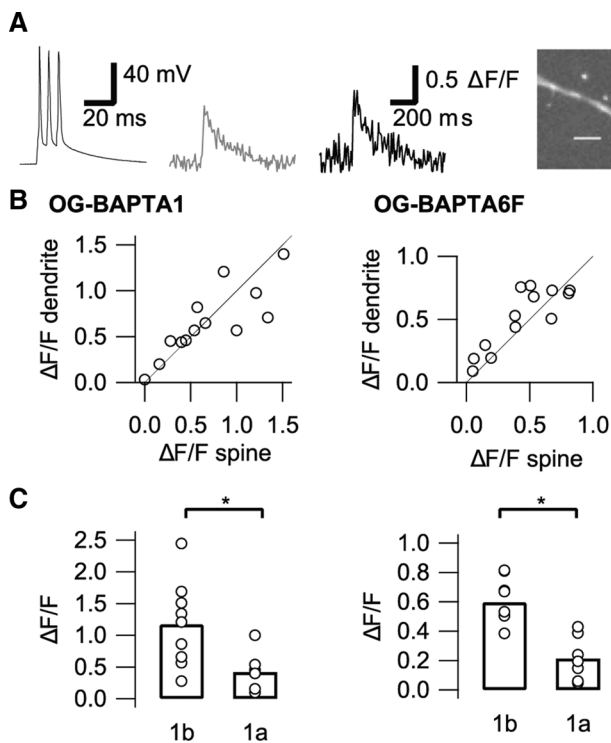


Figure 3. On the single-spine level, backpropagating AP-mediated Ca^{2+} signals also display attenuation in layer 1a. **A**, Left, Time course of the Ca^{2+} signal in spine and dendrite evoked by three APs at 150 Hz. Right, Dendritic branch with analyzed spine and dendrite indicated by black and gray arrows, respectively. Scale bar, 5 μm . **B**, Plot of peak Ca^{2+} signals in dendrites versus corresponding spines evoked by firing of three APs at 150 Hz with OGB1 (left) and OGB6F (right). Spines display peak Ca^{2+} signals comparable with dendrites. **C**, The average peak Ca^{2+} signal evoked by three APs at 150 Hz is significantly larger in layer 1b spines than in layer 1a spines both with OGB1 ($n = 9$ and 6 , respectively; $*p < 0.05$; left) and OGB6F ($n = 8$ and 7 , respectively; $*p < 0.01$; right).

pared with preapplication values ($n = 8$) in individual cells in layer 1a. In layer 1b, the same 4-AP application did not change the amplitude of the Ca^{2+} response (post/pre = 1.08 ± 0.07 , $n = 9$; $p < 0.01$ layer 1a vs layer 1b) (Fig. 2C). Drug-free control experiments yielded post/pre ratios of 0.87 ± 0.02 [$n = 5$ (Fig. 2B); $p < 0.01$ layer 1a drug vs layer 1a control (Fig. 2C)]. The smaller post value indicates a slight rundown of the dendritic Ca^{2+} response during the 15 min waiting period between the two measurements. To investigate the contribution of D-type K^+ channels, which are also affected by high 4-AP concentrations, we tested low concentrations of 4-AP (100 μM) (Kampa and Stuart, 2006). At this 4-AP concentration, affecting primarily D-type K^+ channels, the post/pre ratios were 1.37 ± 0.24 and not significantly different from the drug-free control experiments ($n = 5$; $p > 0.05$, layer 1a drug vs layer 1a control). We conclude that the differential distribution of A-type K^+ channels in the apical dendrite of layer 2 pyramidal cells of the piriform cortex, i.e., higher expression levels in layer 1a than layer 1b, results in the functional compartmentalization of the dendrites into two segments.

Different spine Ca^{2+} signals mediated by action potential backpropagation in layer 1a and layer 1b

Dendritic spines constitute the subcellular compartment in which the actual synaptic contacts that define the input layers are located. The differences between distinct synaptic layers with respect to dendritic Ca^{2+} responses to bAPs were analyzed at

the single-spine level. We initially compared the amplitude of bAP-evoked Ca^{2+} transients in spines and dendrites (Fig. 3A,B). We observed no significant differences between the bAP-mediated Ca^{2+} responses of the two subcellular compartments. Using OGB1, the ratio of the response amplitude between dendrite and spine was 1.03 ± 0.1 ($n = 12$). With OGB6F, this dendrite/spine ratio was 1.44 ± 0.18 ($n = 13$). The trend that somewhat larger dendritic Ca^{2+} transients were observed with the medium-affinity indicator was not statistically significant ($p > 0.05$), and it can be explained by the reduced degree of dendrite–spine diffusion of indicator-bound Ca^{2+} attributable to the lower buffering capacity (Sabatini et al., 2002) (for review, see Higley and Sabatini, 2008). As seen for dendritic transients, the amplitudes of bAP-mediated Ca^{2+} responses were different for spines in the two input layers, with significantly larger responses observed in layer 1b using both OGB1 and OGB6F (Fig. 3C).

Spine Ca^{2+} transients mediated by synaptic stimulation in layer 1a and layer 1b

The next step was to measure Ca^{2+} transients in dendritic spines evoked by subthreshold synaptic stimulation. EPSPs are expected to result in specific and large Ca^{2+} transients in spines relative to dendrites (Yuste and Denk, 1995). Synaptic stimulation resulted in isolated spine Ca^{2+} transients, with dendrite/spine ratios of 0.29 ± 0.07 ($n = 9$) for experiments with OGB1 and 0.32 ± 0.07 ($n = 13$) when OGB6F was used (Fig. 4A,C). These values are in accordance with previously published ratios measured using OGB1 and two-photon imaging (Nevian and Sakmann, 2004). As shown in Figure 4A, synaptic stimulation was synapse specific. The overlay of several single responses (Fig. 4A, bottom) reveals that both successful synaptic transmission and synaptic failures could be detected. This mirrors the probabilistic nature of synaptic transmission at the spine Ca^{2+} level (Yuste and Denk, 1995). Spine Ca^{2+} transients evoked by synaptic stimulation were almost completely blocked after a 5 min application of the NMDAR antagonist D-APV at 50 μM (reduction to $11 \pm 3\%$ of preapplication values, $n = 5$; $p < 0.01$) (Fig. 4B). When comparing the amplitudes of synaptically activated spine Ca^{2+} transients in layer 1a and layer 1b, there was no significant difference observed for either of the Ca^{2+} indicators (OGB1: layer 1b, $0.99 \pm 0.14 \Delta F/F$, $n = 7$; layer 1a, $0.83 \pm 0.12 \Delta F/F$, $n = 4$; $p > 0.05$; OGB6F: layer 1b, $0.6 \pm 0.09 \Delta F/F$, $n = 6$; layer 1a, $0.48 \pm 0.07 \Delta F/F$, $n = 8$; $p > 0.05$) (Fig. 4D).

We observed a large variability of the somatic voltage recorded with the imaged spines (Fig. 4E), based on the variable number and strength of the synapses activated with extracellular stimulation. In most CNS synapses, a single axon constitutes several diffusely distributed synaptic contacts to a given postsynaptic cell (Shepherd, 2004). The anatomical data characterizing the number of synaptic contacts per pair of connected cells is missing for the piriform cortex. Regardless of the underlying axonal projection patterns, the primary relevant concern here is that the coincident activation of several neighboring spines might result in a dendritic depolarization. This would cause additional spine Ca^{2+} influx and result in distortion of the EPSP-mediated signal. AP-mediated Ca^{2+} signals that result in global dendritic depolarization are as large as or larger than the associated spine responses (Fig. 4C). In contrast, the observed EPSP-mediated signals are larger in the spine than in the dendrite (Fig. 4D). This argues against significant dendritic depolarization. In addition, the full-frame scan applied with the spinning disc confocal permits for

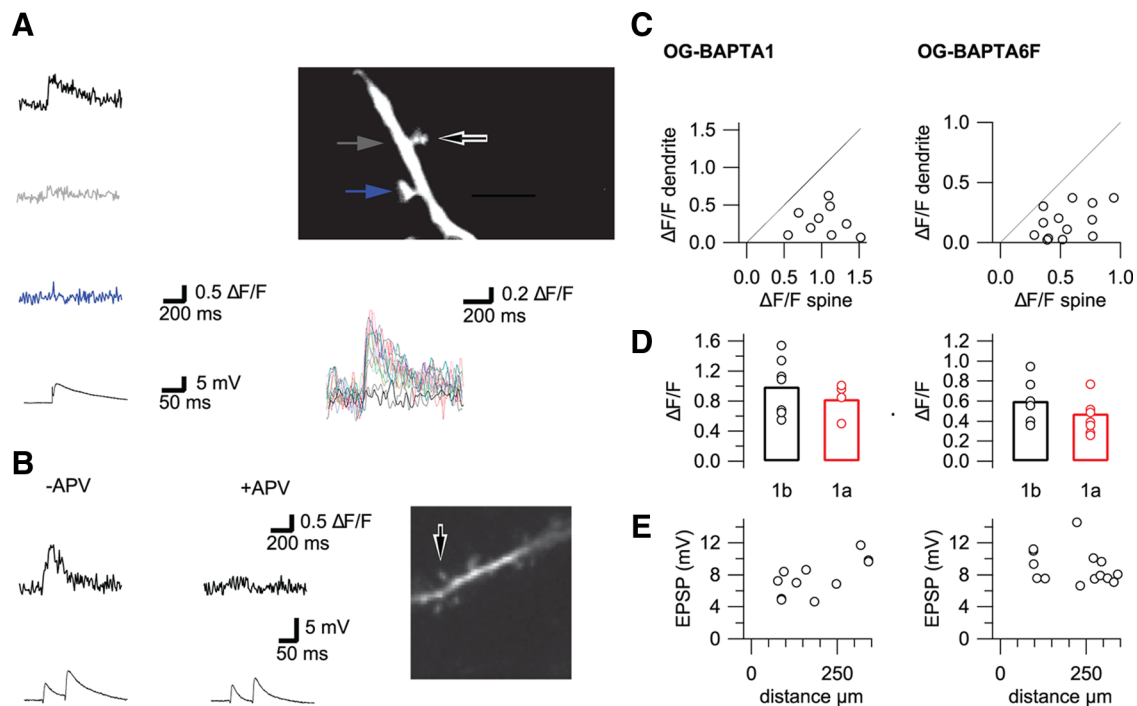


Figure 4. Single-spine Ca^{2+} signals evoked by synaptic stimulation are NMDAR dependent and do not differ between layer 1a and layer 1b. **A**, Left, Time course of EPSP-mediated Ca^{2+} signal in stimulated spine, adjacent dendrite, and unstimulated spine. Top right, Dendritic branch with active spine (black arrow), adjacent dendrite (gray arrow), and inactive spine (blue arrow). This image was acquired with a high-resolution CCD camera different from the CCD camera used for detecting Ca^{2+} signals. Scale bar, $5 \mu\text{m}$. Bottom right, The overlay displays Gaussian filtered time courses of single EPSP-mediated Ca^{2+} signals from the active spine and demonstrates distinguishable synaptic failures. **B**, Left, Time course of EPSP-mediated Ca^{2+} transient in stimulated spine evoked by paired-pulse stimulation at 20 Hz before D-APV application. Middle, Time course of EPSP-mediated Ca^{2+} signal in the same spine after 5 min of $50 \mu\text{M}$ D-APV reveals almost complete block of the spine Ca^{2+} transient. Right, Dendritic branch with analyzed spine (black arrow). Scale bar, $5 \mu\text{m}$. **C**, Plot of peak Ca^{2+} signals in dendrites versus corresponding spines evoked by synaptic stimulation measured with OGB1 (left) and OGB6F (right). During synaptic stimulation, spines exhibit larger peak Ca^{2+} signals than dendrites. **D**, The average peak Ca^{2+} signal in spines evoked by synaptic stimulation is comparable in layer 1b and layer 1a for OGB1 ($n = 7$ and 4 , respectively; $p > 0.05$; left) and OGB6F ($n = 6$ and 8 , respectively; $p > 0.05$; right). **E**, Plot of EPSP amplitude versus distance of the corresponding imaged spine from the soma. Left, Spines recorded with OGB1. Right, Spines recorded with OGB6F.

scanning of a larger dendritic segment. Significant dendritic voltage changes were further excluded by the absence of voltage change-mediated Ca^{2+} transients in dendritic segments adjacent to unstimulated spines.

Calcium transients measured during subsequent presynaptic activation and postsynaptic bursting reveal different integrative properties of layer 1a and layer 1b spines

We demonstrated that, in layer 2 pyramidal cells of the piriform cortex, the spine Ca^{2+} influx during synaptic activation is mediated by NMDARs (Fig. 4B). LTP can be induced in pyramidal cells when the presynaptic firing is followed by postsynaptic spiking at a time interval of up to 50 ms (Magee and Johnston, 1997; Markram et al., 1997; Bi and Poo, 1998; Debanne et al., 1998) (for review, see Kampa et al., 2007). During LTP induction, bAPs can boost the spine Ca^{2+} response by depolarization-mediated release of the NMDAR Mg^{2+} block (Koester and Sakmann, 1998; Kampa et al., 2004; Nevian and Sakmann, 2004, 2006). The integration of presynaptic and postsynaptic firing in spines in the layer 1a and layer 1b dendritic compartments was analyzed. During presynaptic and postsynaptic stimulation at a time interval of 10 ms, we computed the average amplitude of the spine Ca^{2+} transient. Under these conditions, the high-affinity indicator OGB1 was already partially saturated, so the medium-affinity indicator OGB6F was used. The amplitude in layer 1b exceeded that of layer 1a by almost twofold (layer 1b, $1.62 \pm 0.38 \Delta F/F$, $n = 6$ vs layer 1a, $0.84 \pm 0.12 \Delta F/F$, $n = 7$; $p < 0.01$) (Fig. 5A–C). Supralinear summation means that coincident synaptic stimula-

tion and postsynaptic firing lead to a larger Ca^{2+} response than expected from the linear sum of the isolated responses (Fig. 5A, B). Associative layer 1b spines exhibit a significantly larger degree of supralinearity when compared with sensory layer 1a spines (layer 1b, 1.42 ± 0.05 , $n = 6$ vs layer 1a, 1.15 ± 0.01 , $n = 7$; $p < 0.05$) (Fig. 5A–C). The voltage-dependent relief of the Mg^{2+} block of the NMDAR is the underlying mechanism for the supralinear summation of the spine Ca^{2+} response by coincident presynaptic and postsynaptic firing (Nevian and Sakmann, 2004). We wanted to ensure that the initial EPSP-mediated voltage changes did not have an impact on the linearity index. We therefore plotted the depolarization, mediated by the EPSP, against the linearity index measured in individual experiments, and no correlation was observed (Fig. 5C).

Spikes were delivered as 150 Hz triplets to increase the efficiency of action potential backpropagation to distal dendrites (for review, see Kampa et al., 2007). These postsynaptic bursts have been observed with sensory and associative inputs to layer 2/3 pyramidal cells in the piriform cortex *in vitro* (Suzuki and Bekkers, 2006) and *in vivo* (Wilson, 1998). However, isolated layer 1a stimulation has been shown recently to recruit prominent perisomatic feedforward inhibition, and single APs are the predominant cellular output during suprathreshold extracellular stimulation in layer 1a (Luna and Schoppa, 2008). We asked how this tightly controlled output mode affects the integration of presynaptic and postsynaptic firing in layer 1b spines. Pairing an EPSP with one or three bAPs, the amplitudes and linearity indices of spine Ca^{2+} responses were

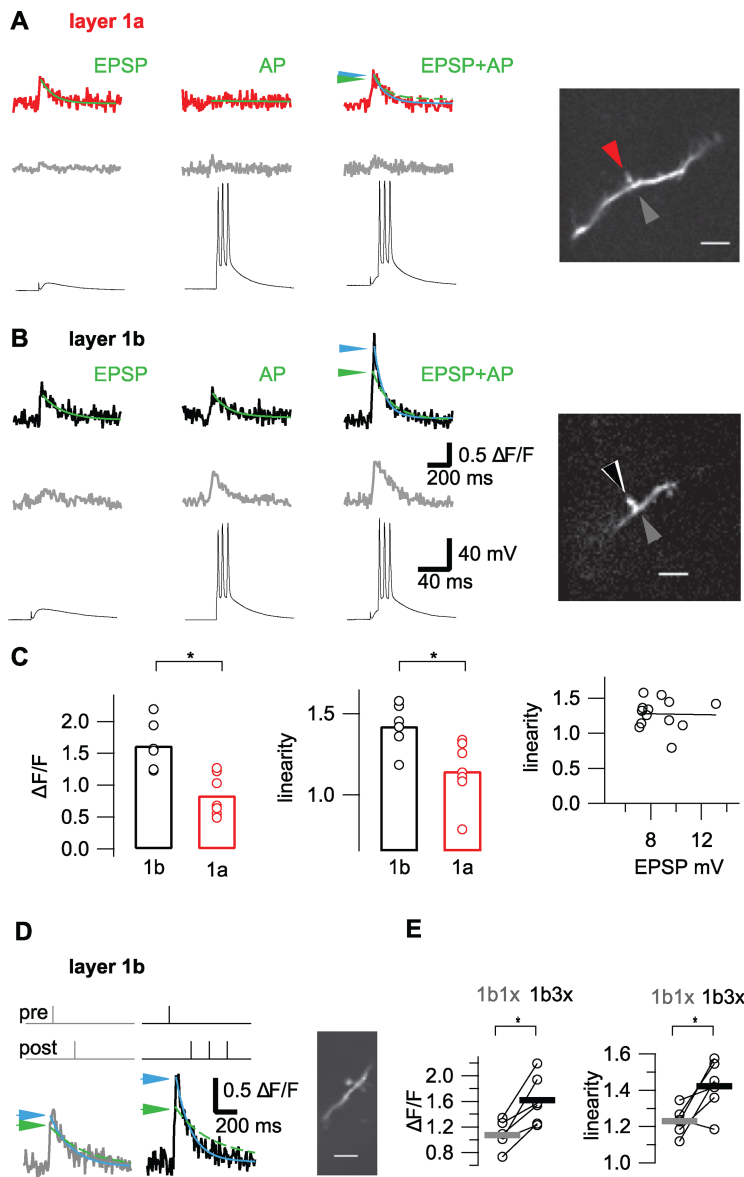


Figure 5. Pairing of EPSPs and APs results in supralinear increase of spine Ca^{2+} signals in layer 1b only. **A**, Left, Comparison of Ca^{2+} signals in spines (top) and adjacent dendrites (middle) evoked by an EPSP, three APs at 150 Hz, and a pairing sequence in which an EPSP is followed by three APs at 150 Hz with a Δt of 10 ms (bottom) in a layer 1a spine. The green lines are monoexponential fits of the EPSP and AP-mediated spine Ca^{2+} signals, and the fit of the pairing sequence is represented by the blue line. The dotted green line in the trace of the pairing sequence is the linear sum of the fits of the isolated EPSP and AP. The arrows point at the peaks of the two fits. Right, Dendritic branch with analyzed spine (red arrow) and adjacent dendritic segment (gray arrow). Scale bar, $5 \mu\text{m}$. This example displays almost linear addition of the spine Ca^{2+} signal during pairing of the EPSP with the APs. **B**, Left, Comparison of Ca^{2+} signals in spines and adjacent dendrites evoked by EPSPs, three APs at 150 Hz, and a pairing sequence consisting of an EPSP followed by three APs at 150 Hz with a Δt of 10 ms in a layer 1b spine. The color code of the monoexponential fits is identical to **A**. Right, Dendritic branch with analyzed spine (black arrow) and adjacent dendritic segment (gray arrow). Scale bar, $5 \mu\text{m}$. This example displays supralinear addition of the spine Ca^{2+} signal during pairing of the EPSP with the APs. **C**, Left, When pairing an EPSP with three APs at 150 Hz at a Δt of 10 ms, the averaged amplitudes of the Ca^{2+} signals in layer 1b spines ($n = 6$) are significantly larger than in layer 1a spines ($n = 7$; $*p < 0.01$). Middle, Layer 1b spines ($n = 6$) display a significantly larger supralinear addition of EPSPs and APs when compared with layer 1a spines ($n = 7$; $p < 0.05$). Right, Plot of the linearity indices measured in spines versus the corresponding EPSP amplitudes. The linearity indices in spines are independent of the EPSP amplitudes. **D**, Left, Time course of spine Ca^{2+} signals in layer 1b spines during pairing of an EPSP with one AP (EPSP–AP sequence; see schematic illustration on top). The blue line represents the monoexponential fit of the paired EPSP–AP sequence, and the green line represents the linear sum of the fits of the isolated EPSP and AP. The arrows point at the peak amplitude of the fits. Middle, Time course of Ca^{2+} signals in layer 1b spines during pairing of an EPSP with three APs at 150 Hz (EPSP–three AP sequence; see schematic illustration on top). The color code of the monoexponential fits is identical to the left. Comparison reveals a larger supralinear addition of the spine Ca^{2+} signal when the EPSP is followed by three APs instead of one AP. Right, Dendritic branch with analyzed spine. Scale bar, $5 \mu\text{m}$. **E**, Left, Plot of the peak Ca^{2+} signals from spines stimulated with paired EPSP–AP and EPSP–three AP sequences in layer 1b ($n = 6$). The amplitude is significantly larger when the EPSP is paired with three APs ($*p < 0.05$). Right, Plot of the linearity indices from spines stimulated with EPSP–AP and EPSP–three AP sequences in layer 1b ($n = 6$). The linearity index is significantly larger when the EPSP is paired with three APs ($*p < 0.05$).

compared (Fig. 5D). The average spine Ca^{2+} signal increased from $1.07 \pm 0.09 \Delta F/F$ for one AP to $1.62 \pm 0.15 \Delta F/F$ for three APs ($n = 6$; $p < 0.05$) (Fig. 5E). The linearity index changed from an average value of 1.23 ± 0.03 for one AP to 1.42 ± 0.05 for three APs ($n = 6$; $p < 0.05$) (Fig. 5E).

Pathway-specific LTP induction

In pyramidal cells in CA1 and the neocortex, the supralinear spine Ca^{2+} responses are considered to be the elementary building blocks of LTP induction, with paradigms based on pairing EPSPs with subsequent bursts of APs (Pike et al., 1999; Kampa et al., 2006; Letzkus et al., 2006; Nevian and Sakmann, 2006). We wanted to relate the observed differences between spine Ca^{2+} responses in layer 1a and those in layer 1b to the induction of LTP. For this purpose, LTP was induced in both layers using a stimulation protocol based on the stimuli displayed in Figure 5. To ensure pathway specificity of our LTP measurements, we first established the selective synaptic stimulation of layer 1a and layer 1b synapses on apical dendrites of layer 2 pyramidal neurons. Electrodes were placed at the layer 2/layer 1b border for 1b stimulation and at the LOT/layer 1a border for 1a stimulation. It has been established previously that presynaptic GABA_B receptors are exclusively expressed on layer 1b synapses. It follows from this that application of the GABA_B agonist baclofen selectively diminishes layer 1b inputs, leaving layer 1a essentially unaffected (Tang and Hasselmo, 1994; Franks and Isaacson, 2005). In a subset of our LTP experiments, we confirmed the selective stimulation of the two different pathways by postexperimental application of $30 \mu\text{M}$ baclofen. Between 3 and 4 min after baclofen application, we observed a reduction of layer 1b inputs to $17.8 \pm 2.7\%$ ($n = 7$) of baseline values. The layer 1a inputs remained stable at $99 \pm 9.3\%$ ($n = 6$) of baseline level ($p < 0.01$) (Fig. 6B). Selective stimulation of layer 1a by pharmacological block of layer 1b synapses with baclofen has been demonstrated previously (Franks and Isaacson, 2005; Poo and Isaacson, 2007); however, it is important to note that GABA_B receptors activate dendritic K^+ conductances and inhibit voltage-gated calcium channels (VGCCs) in the postsynaptic cell (Pérez-García et al., 2006). The pharmacological isolation approach thus activates mechanisms that diminish layer 1a Ca^{2+} responses evoked by bAPs and is therefore unsuited for our

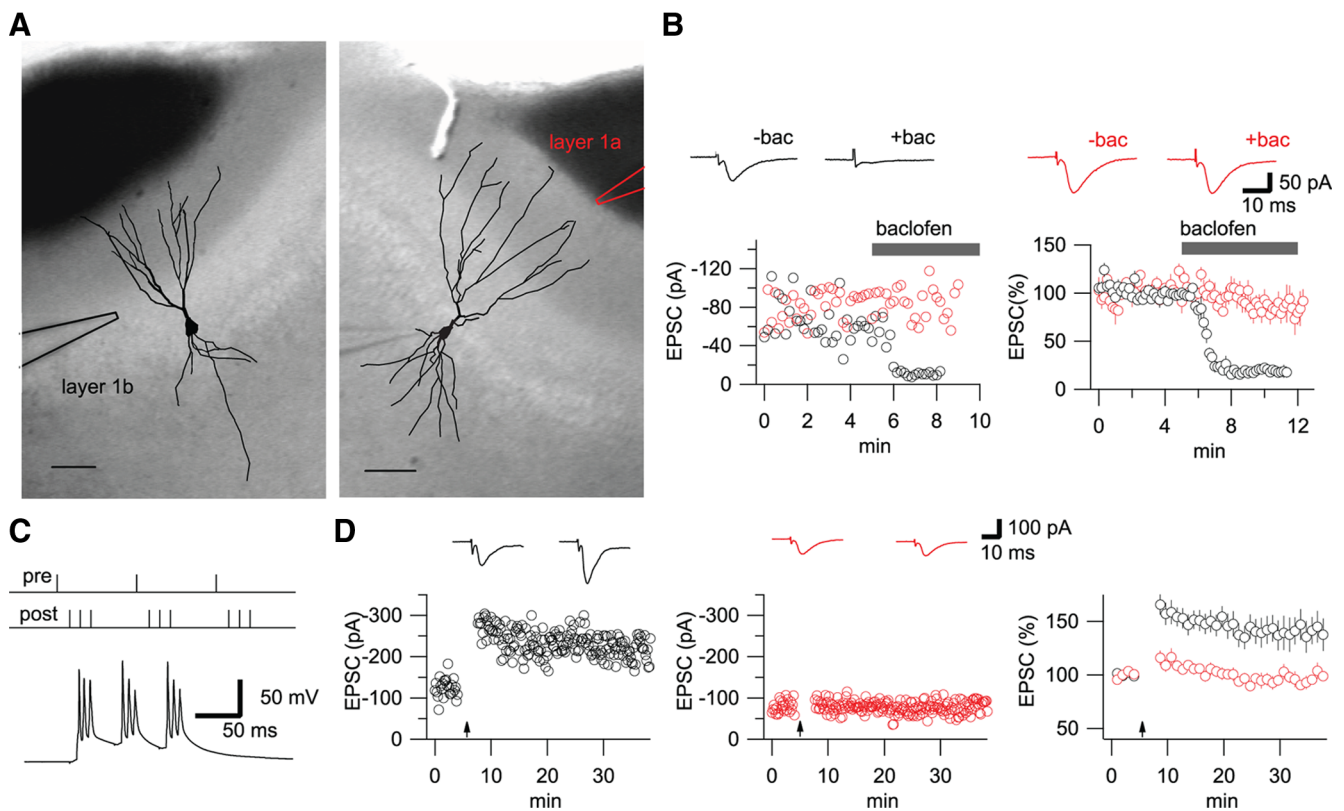


Figure 6. Pairing EPSPs with postsynaptic AP bursts only induces LTP in layer 1b. **A**, Left, Camera lucida reconstruction of recorded layer 2 pyramidal cell in the anterior piriform cortex projected onto a DIC image of the acute brain slice. The stimulation electrode positioned in layer 1b is highlighted in black. Right, Camera lucida reconstruction of recorded layer 2 pyramidal cell in the anterior piriform cortex projected onto a DIC image of the acute brain slice. The stimulation electrode positioned in layer 1a is highlighted in red. Scale bars correspond to 100 μm . **B**, Top left, Corresponding evoked EPSCs before and 3 min after baclofen (bac) application from the cell in the left panel of **A** demonstrates block of evoked EPSCs by baclofen. Top right, Evoked EPSC before and 3 min after baclofen application from the cell in the **A**. Compared with the layer 1b stimulation in the left, the EPSC evoked by layer 1a stimulation is unaffected by blocking GABA_B receptors. Bottom left, Time course of evoked EPSC amplitudes for the cells in the left panel of **A** (black) and the right panel of **A** (red), demonstrating the exclusive effect of baclofen on layer 1b. Bottom right, Time course of normalized amplitudes of layer 1a ($n = 6$) and layer 1b ($n = 7$) inputs in response to baclofen application. GABA_B receptor block via baclofen results in selective reduction of layer 1b EPSCs ($p < 0.01$). **C**, Top, Schematic illustration of the LTP induction protocol consisting of 30 bursts of EPSP triplets at 20 Hz followed by a 150 Hz triple AP burst 8 ms after each EPSP. Bottom, Voltage trace of a typical induction stimulus. **D**, Bottom left, Time course of EPSC amplitude changes induced by the LTP induction protocol (arrow) in a layer 1b input. Top left, Corresponding averaged EPSCs 4 min before and 20–25 min after LTP induction in layer 1b (black). Bottom middle, Time course of EPSC amplitude changes induced by the LTP induction protocol (arrow) in a layer 1a input. Top middle, Corresponding averaged EPSCs 4 min before and 20–25 min after LTP induction in layer 1a (red). Right, Time course of normalized EPSC amplitude changes induced by the LTP induction protocol (arrow) in layer 1a ($n = 7$; red) and layer 1b ($n = 10$; black) demonstrating the significantly larger potentiation in layer 1b ($p < 0.05$).

study. The observed selective reduction of layer 1b inputs during baclofen application demonstrates that pathway-specific stimulation can be achieved with stimulation electrode placement alone (Fig. 6A,B).

LTP was induced by presynaptic stimulation that resulted in EPSPs paired with subsequent postsynaptic triple AP bursts at a time interval of 8 ms. The EPSP–triple AP sequences were delivered 30 times every 5 s in 20 Hz triplets (Fig. 6C). The 20 Hz input pattern matches the beta oscillations reported for odor-evoked synaptic currents in the piriform cortex (Poo and Isaacson, 2009). Using the paradigm displayed in Figure 6C on both layer 1b and layer 1a inputs, we successfully induced LTP in layer 1b but failed to induce LTP in layer 1a (Fig. 6D). Between 20 and 25 min after LTP induction, cells stimulated in layer 1b were potentiated at an average value of $138.6 \pm 13\%$ ($n = 10$) of preinduction baseline. This was significantly larger than that after layer 1a stimulation, in which cells did not show any potentiation: the EPSC amplitude was $97 \pm 6\%$ ($n = 7$) of baseline values ($p < 0.05$).

Rescue of distal layer 1a LTP by enhanced AP backpropagation

We next analyzed the effect of enhanced AP backpropagation and the resulting change in intracellular Ca^{2+} on the induction of

distal LTP. Blocking A-type K^+ conductances with 4 mM 4-AP substantially reduces the weak distal depolarization during bAP firing and enhances distal voltage-mediated Ca^{2+} influx (Fig. 2). Using our EPSP–triple AP-based LTP induction paradigm in the presence of 4-AP, distal LTP could be evoked. Between 15 and 20 min after LTP induction, layer 1a inputs were potentiated at an average of $143 \pm 18\%$ ($n = 8$) of preinduction baseline values (Fig. 7A,C). In contrast, with the EPSP-based induction protocol in 4-AP, and also with the EPSP–triple AP-based layer 1a LTP induction protocol without 4-AP, cells exhibited no potentiation. The EPSC amplitude was $68 \pm 10\%$ ($n = 7$) and $95 \pm 13\%$ ($n = 8$) of baseline values, respectively ($p < 0.01$ and $p < 0.05$) (Fig. 7C). This demonstrates the instructive role of bAP-associated distal dendritic depolarization and the associated increase in the distal Ca^{2+} response for LTP in layer 1a.

In layer 1b, bursting is a prerequisite for plasticity induction

We examined the induction of LTP in different layers using postsynaptic AP triplets. As described previously, we compared the effect of different output modes on the integration of presynaptic and postsynaptic firing in layer 1b spines with respect to the associated spine Ca^{2+} responses (Fig. 5D). We subsequently de-

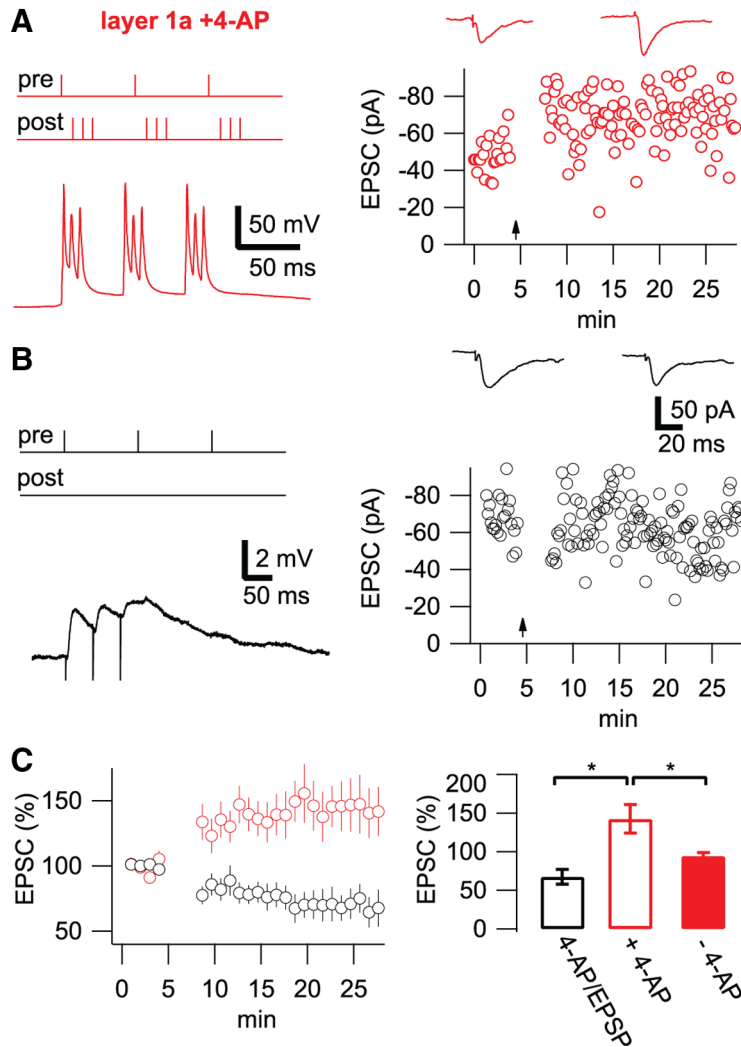


Figure 7. LTP in layer 1a can be induced when bAPs are amplified in layer 1a using 4-AP. **A**, Left, Schematic illustration of the LTP induction protocol in 4-AP and voltage trace of a typical induction stimulus (top). Right bottom, Time course of EPSC amplitude changes induced by the LTP induction protocol (arrow) in a layer 1a input in 4-AP. Right top, Corresponding averaged EPSCs 4 min before and 15–20 min after LTP induction in layer 1a. **B**, Left, Schematic illustration of the control protocol in 4-AP consisting of 30 bursts of EPSP triplets at 20 Hz and corresponding voltage trace (top). Right bottom, Time course of EPSC amplitude changes induced by the EPSP-only control protocol (arrow) in layer 1a in a representative cell. Right top, Corresponding averaged EPSCs 4 min before and 15–20 min after EPSP-only control protocol in layer 1a. **C**, Left, Time course of normalized EPSC amplitude changes in 4-AP induced by the induction protocol based on pairing EPSPs with triple APs ($n = 8$; red) and the EPSP-only control protocol ($n = 7$; black) in layer 1a. Right, Bar diagram displays the averaged EPSC amplitudes at 15–20 min after different induction protocols normalized to preinduction values. Pairing EPSPs with triple APs in 4-AP for induction in layer 1a leads to significantly larger LTP when compared with EPSPs paired with triple APs in 1a without 4-AP and the EPSP-only control protocol in 4-AP (* $p < 0.05$ and * $p < 0.01$, respectively).

terminated whether or not these differences in the amplitudes of spine Ca^{2+} transients also translated into differences in synaptic plasticity induction. First, we used the LTP induction protocol based on pairing EPSPs with three APs but prevented postsynaptic Ca^{2+} increase with application of 30 mM intracellular BAPTA. This resulted in a block of LTP, with an EPSP amplitude of $92 \pm 5\%$ of baseline values ($n = 7$; $p < 0.05$) (Fig. 8A,D). Another method used for reducing the spine Ca^{2+} transient was the application of a pairing paradigm with one AP instead of three (Figs. 5D, 7B). Under these conditions, LTP could not be induced: the EPSC amplitude was $79 \pm 14\%$ of preinduction baseline values ($n = 5$) (Fig. 8D) and significantly smaller than potentiation levels after the induction with three APs ($p < 0.01$). As a control

experiment, EPSPs alone were used for LTP induction (Fig. 8C). The EPSC amplitude was $90 \pm 10\%$ of the preinduction value ($n = 6$). This result is not significantly different from that after LTP induction with a protocol based on the pairing of an EPSP with a single AP or with three APs in the presence of 30 mM intracellular BAPTA ($p > 0.05$) (Fig. 8D). However, the difference was significant when comparing these results with the induction protocol based on pairing EPSPs with three APs in the absence of BAPTA ($p < 0.05$) (Fig. 8D).

We next tested whether or not short high-frequency bursts could be evoked by coincident single-pulse stimulation of layer 1a and layer 1b inputs. Strong perisomatic inhibition, which occurs as a result of extracellular stimulation, resulted in isolated APs. For this reason, we proceeded under conditions of reduced inhibition (2 μM gabazine). Single subthreshold pulses in layer 1a and 1b were paired at different time intervals. Coincident subthreshold activation of layer 1a and layer 1b at time intervals between -10 and $+10$ ms resulted in bursts of two to four APs. The first three spikes of the bursts were in the frequency range of ~ 100 Hz. Longer time intervals (-100 , -50 , 50 , and 100 ms) did not result in bursting (Fig. 8E,D). It is important to note that suprathreshold activation of isolated layer 1a and layer 1b inputs resulted in similar bursts. In neocortical layer 5 pyramidal cells, bursting has also been evoked by pairing an EPSP with a bAP (Larkum et al., 1999b). We also wanted to test whether subthreshold depolarization by a layer 1b EPSP could result in bursting when combined with a somatically evoked spike under conditions of reduced inhibition. Despite the strong effect of coincident subthreshold synaptic activation between -10 and $+10$ ms, pairing at similar time intervals did not yield any bursts when an EPSP was paired with a somatically evoked bAP (supplemental Fig. S1, available at www.jneurosci.org as supplemental material).

Discussion

Dendritic compartmentalization determined by the synaptic input layer

We compared dendritic segments in the proximal associative input layer 1b with the distal sensory input layer 1a. In layer 1a, the amplitude of bAP-mediated Ca^{2+} signals decreased. In neocortical pyramidal cells, this distance-dependent decrease can be overcome by burst firing-mediated distal Ca^{2+} spikes (Larkum et al., 1999a; Waters et al., 2003; Kampa and Stuart, 2006; Larkum et al., 2007). In layer 2 pyramidal cells of the piriform cortex, we did not observe such a regenerative mechanism, which is comparable with the CA1 pyramidal cell in the hippocampus (for

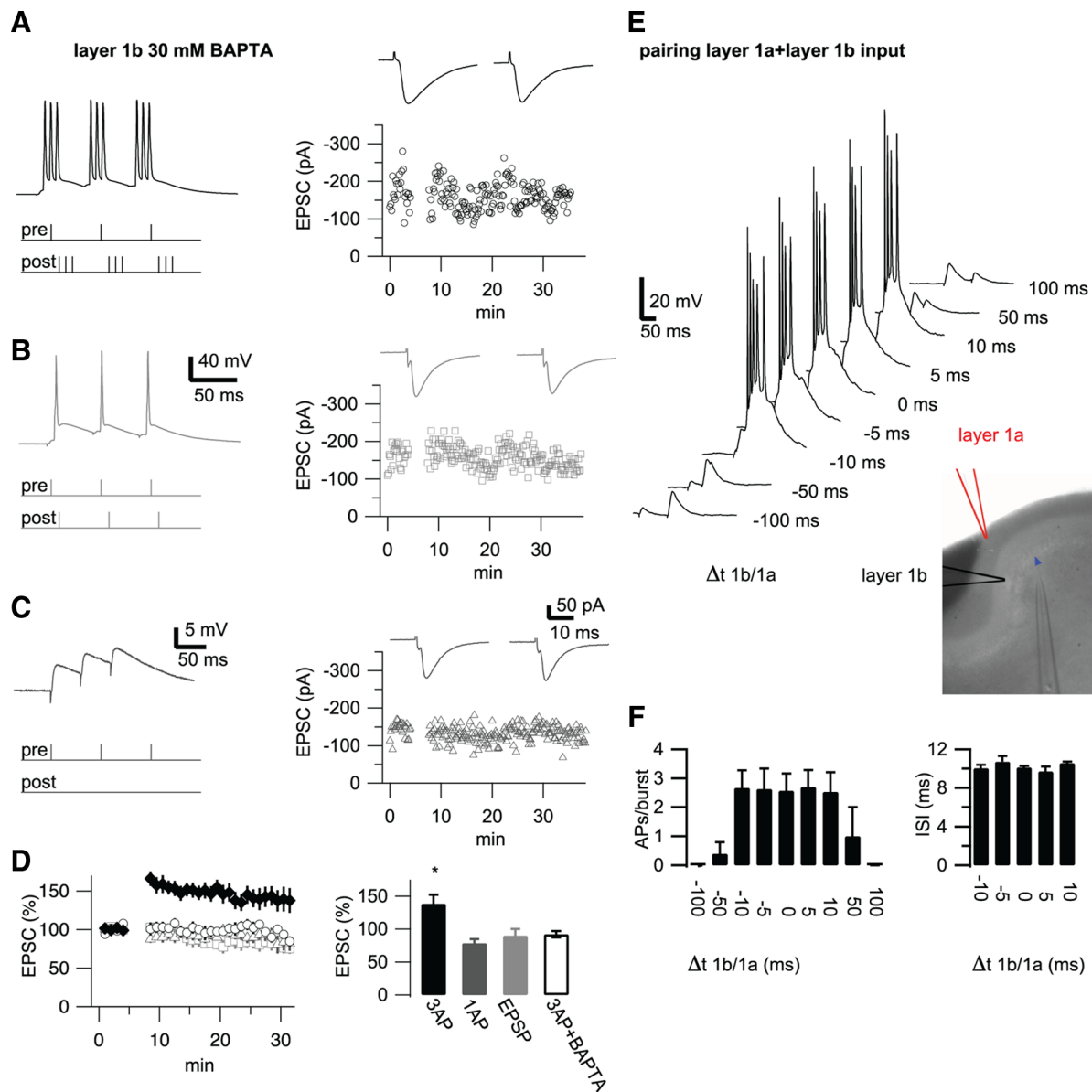


Figure 8. Pairing EPSPs with postsynaptic single APs does not result in layer 1b LTP. **A**, Left, Schematic illustration of the LTP induction protocol with 30 mM intracellular BAPTA and voltage trace of a typical induction stimulus (top). Bottom right, Time course of EPSC amplitude changes induced by the induction protocol (arrow) based on pairing EPSPs with three APs in layer 1b in a representative cell with 30 mM intracellular BAPTA. Top right, Corresponding averaged EPSCs 4 min before and 20–25 min after induction in layer 1b. **B**, Left, Schematic illustration of the induction protocol consisting of 30 bursts of EPSP triplets at 20 Hz followed by a single AP 8 ms after each EPSP and corresponding voltage trace (top). Bottom right, Time course of EPSC amplitude changes induced by the induction protocol (arrow) based on pairing EPSPs with single APs in layer 1b in a representative cell. Top right, Corresponding averaged EPSCs 4 min before and 20–25 min after induction in layer 1b. **C**, Left, Schematic illustration of the control protocol consisting of 30 bursts of EPSP triplets at 20 Hz and corresponding voltage trace (top). Bottom right, Time course of EPSC amplitude changes induced by the EPSP-only control protocol (arrow) in layer 1b in a representative cell. Top right, Corresponding averaged EPSCs 4 min before and 20–25 min after administration of the EPSP-only control protocol. **D**, Left, Time course of normalized EPSC amplitude changes induced by the induction protocol based on pairing EPSPs with three APs ($n = 10$; black diamonds), three APs and intracellular BAPTA ($n = 6$; black circles), single APs ($n = 5$; light gray squares), and the EPSP-only control protocol ($n = 6$; dark gray triangles) in layer 1b. Right, Bar diagram displays the averaged EPSC amplitudes at 20–25 min after different induction protocols normalized to preinduction values. LTP based on pairing EPSPs with three APs in layer 1b is significantly larger when compared with pairing EPSPs with single APs, the EPSP-only protocol, and the EPSP–three AP protocol with 30 mM intracellular BAPTA ($*p < 0.05$). **E**, The waterfall plot represents one of six anterior piriform cortex pyramidal cells in which layer 1a and layer 1b inputs as indicated in the inset were stimulated with different time intervals. Between -10 (layer 1b before layer 1a) and $+10$ (layer 1a before layer 1b) ms, we observed burst firing of subthreshold signals, which was not present at longer time intervals. **F**, Left, The bar graph indicates the number of APs/burst for the different time intervals ($n = 3$ to 6). Right, The bar graph displays the average interspike intervals (ISI) of the first three spikes in a burst. Four of six cells displayed more than two subsequent spikes.

review, see Sjöström et al., 2008). It is tempting to speculate that the palaeocortex, like its phylogenetic relative, the three-layered amphibian cortex in the turtle (Larkum et al., 2008), does not use supralinear Ca^{2+} spikes for dendritic signal integration. This would render AP burst-mediated Ca^{2+} spikes an evolutionary younger mechanism, which is an exclusive property of the neocortex.

A failure of the active spread of the voltage signal mediates the distal attenuation of bAP-mediated Ca^{2+} transients in CA1 pyramidal cells in the hippocampus and in basal dendrites of layer 5 pyramidal cells. However, there is substantial distal expression of voltage-gated Ca^{2+} channels. The underlying mechanism for this is the differential distribution of the depolarization-activated A-type K^{+} -channels, which provides an electrical shunt (Hoff-

man et al., 1997; Kampa and Stuart, 2006; Gasparini et al., 2007). We observed a similar situation in apical dendrites of layer 2 pyramidal cells in the piriform cortex: the pharmacological block of A-type K^+ conductances resulted in a significant increase in the amplitude of bAP-mediated Ca^{2+} signals in layer 1a, and we demonstrated that expression levels of Kv4.2 and Kv4.3 (the subunits underlying dendritic A-type conductances) are higher in layer 1a than in layer 1b. Finally, failure of voltage propagation is documented using the coincidence detection mechanism of the NMDAR as a reporter (Kampa et al., 2004; Nevian and Sakmann, 2004). This second readout of dendritic depolarization is of special importance, because the distance-dependent amplitude of bAP-mediated Ca^{2+} signals may be affected by factors different from the spread of the voltage signal.

Spines in different input layers of the apical dendrite constitute distinct plasticity compartments based on integrative dendritic properties

For LTP induction based on the pairing of presynaptic and postsynaptic activity in mammalian principal neurons, the presynaptic cell must fire milliseconds before the postsynaptic cell (Magee and Johnston, 1997; Markram et al., 1997; Bi and Poo, 1998; Debanne et al., 1998) (for review, see Kampa et al., 2007). Spine Ca^{2+} transients evoked by these pairing sequences are the elementary building block of associated induction protocols (Nevian and Sakmann, 2006) (for review, see Sjöström et al., 2008). Our data suggest that the electrical properties of layer 2 pyramidal cell dendrites in the piriform cortex result in single-spine Ca^{2+} signals during LTP induction that differ between layers 1a and 1b. Factors determining spine Ca^{2+} reduction in layer 1a are (1) the failure of the bAP to relieve the Mg^{2+} block of the NMDAR, and (2) a smaller VGCC-mediated Ca^{2+} influx. In distal dendrites of neocortical and hippocampal CA1 pyramidal cells, the induction of LTP by pairing EPSPs with subsequent APs is impaired (Golding et al., 2002; Letzkus et al., 2006; Sjöström and Häusser, 2006). Consistent with this, we were only able to induce LTP by pairing EPSPs with subsequent AP bursts in the proximal layer 1b. This effect on synaptic plasticity underscores the functional relevance of our observation that spine Ca^{2+} signals reflect an input layer-specific dendritic compartmentalization.

Impairment of distal LTP induction complements previous findings on impaired expression of layer 1a LTP

After a brief postnatal critical period, NMDAR-dependent LTP in layer 2/3 cells of the anterior piriform cortex is more pronounced in the associative layer 1b than in the sensory layer 1a synapses (Jung et al., 1990a,b; Kanter and Haberly, 1990; Franks and Isaacson, 2005; Poo and Isaacson, 2007). Looking for a mechanistic explanation for this phenomenon, we observed striking differences between layer 1a and layer 1b in the spine Ca^{2+} transients underlying LTP induction. These findings constitute a complementary extension of a previously reported mechanism for the expression of LTP. Franks and Isaacson (2005) reported a selective reduction of silent synapses in layer 1a after a postnatal critical period. However, synapses do not have to be silent to undergo LTP (Matsuzaki et al., 2004; Bagal et al., 2005; Harvey and Svoboda, 2007) (for review, see Kerchner and Nicoll, 2008). It is also important to note that layer 1a LTP can be rescued by low extracellular $[Mg^{2+}]$ (Jung et al., 1990b). Low extracellular $[Mg^{2+}]$ releases the Mg^{2+} block of the NMDAR, which compensates for a reduction in layer 1a depolarization and results in elevated postsynaptic $[Ca^{2+}]$ during LTP induction. When blocking A-type K^+ channels with 4-AP, pairing EPSPs with bAPs

readily induced layer 1a LTP. This was not possible in controls using EPSPs without bAPs, indicating that the enhanced AP backpropagation elevates postsynaptic Ca^{2+} , which rescues layer 1a LTP.

LTP induction is a complex phenomenon with a plethora of synapse-specific underlying mechanisms. It is conceivable that there are additional differences in the molecular machinery of layer 1a and layer 1b presynaptic and postsynaptic architecture that result in different levels of induction and expression of synaptic plasticity. Synapses projecting to layer 1a and layer 1b inputs have entirely different origins (mitral/tufted cells in the olfactory bulb for layer 1a and piriform cortex pyramidal cells, associative connections from other cortical areas for layer 1b). Moreover, electron microscopic analysis of layer 1a and layer 1b synapses indicated striking morphological differences (Haberly and Behan, 1983).

Coincidence detection of presynaptic and postsynaptic firing by the NMDAR also reports the cellular output mode

In associative layer 1b spines of piriform cortex layer 2 pyramidal cells, postsynaptic bursting-mediated Ca^{2+} signals are a prerequisite for LTP induction. Pairing EPSPs with subsequent bursts of APs has also been shown to be a prerequisite for LTP induction in pyramidal cells in CA1 and the neocortex (Pike et al., 1999; Kampa et al., 2006; Letzkus et al., 2006; Nevian and Sakmann, 2006). The most obvious reason for the requirement of bursting for LTP induction is the additional Ca^{2+} provided by a larger degree of VGCC activation. On the level of single-spine EPSP-AP integration, our data suggests an additional mechanism: one AP does not fully relieve the Mg^{2+} block of the NMDAR, resulting in relatively small supralinearity ratios. Additional APs increase the supralinear Ca^{2+} influx mediated by the NMDAR. The gain of this coincidence detector is therefore set in a range that also reports the output mode of the cell at the level of single-spine integration.

Functional implications for learning in the piriform cortex network

The lack of LTP in layer 1a synapses after the critical period has been assumed to result in the hardwiring of sensory olfactory bulb inputs to the piriform cortex (Franks and Isaacson, 2005). We document that this concept of hardwiring is supported by a functional compartmentalization of the apical dendritic tree, based on intrinsic electrical properties that influence plasticity-inducing spine Ca^{2+} transients. This underscores the importance of dendritic excitability for LTP induction (Magee and Johnston, 1997) (for review, see Sjöström et al., 2008).

The potentiation of associative EPSPs depends not only on the strength of the excitatory inputs but also on the output mode of the cell. The output mode is regulated by the balance of excitation and inhibition resulting from synaptic and intrinsic currents. Luna and Schoppa (2008) observed a strong perisomatic inhibitory control exerted by single GABAergic interneurons. One could envision a mechanism in which GABAergic interneurons control the plasticity of excitatory synapses by controlling the output mode of the cell. The net result is a high threshold for the amplification of associative synapses, a mechanism promoting network stability. Interestingly, olfactory rule learning, a behavioral state that corresponds to enhanced learning capability, is associated with a temporary increase in general intrinsic excitability in the piriform cortex (for review, see Barkai and Saar, 2001). Neuromodulation by cholinergic projections promotes this increase in excitability and learning capability (Saar et al.,

2001). One could assume a connection between enhanced learning and facilitated synaptic strengthening. A previous enhancement of burst firing during rule learning would then increase the probability of synaptic strengthening in associative layer 1b networks.

A-type K^+ channel-mediated currents are dynamically regulated by LTP, inducing synaptic activation patterns. The NMDAR-dependent enhancement of synaptic strength results in a hyperpolarized shift of A-type K^+ channel inactivation (Frick and Johnston, 2005) and the internalization of Kv4.2 subunits (Kim et al., 2007). It is interesting to speculate that similar mechanisms could facilitate layer 1a LTP. In addition, neuromodulators such as acetylcholine or noradrenalin reduce A-type K^+ channel-mediated currents, promoting the backpropagation of APs into distal dendritic compartments (Hoffman and Johnston, 1999). One could therefore envision a softening of the hardwiring of layer 1a connections that occurs after the critical period and during the learning-associated neuromodulatory network states gating layer 1a synaptic plasticity.

References

- Bagal AA, Kao JP, Tang CM, Thompson SM (2005) Long-term potentiation of exogenous glutamate responses at single dendritic spines. *Proc Natl Acad Sci U S A* 102:14434–14439.
- Barkai E, Saar D (2001) Cellular correlates of olfactory learning in the rat piriform cortex. *Rev Neurosci* 12:111–120.
- Bi GQ, Poo MM (1998) Synaptic modifications in cultured hippocampal neurons: dependence on spike timing, synaptic strength, and postsynaptic cell type. *J Neurosci* 18:10464–10472.
- Birnbaum SG, Varga AW, Yuan LL, Anderson AE, Sweatt JD, Schrader LA (2004) Structure and function of Kv4-family transient potassium channels. *Physiol Rev* 84:803–833.
- Debanne D, Gähwiler BH, Thompson SM (1998) Long-term synaptic plasticity between pairs of individual CA3 pyramidal cells in rat hippocampal slice cultures. *J Physiol* 507:237–247.
- Franks KM, Isaacson JS (2005) Synapse-specific downregulation of NMDA receptors by early experience: a critical period for plasticity of sensory input to olfactory cortex. *Neuron* 47:101–114.
- Frick A, Johnston D (2005) Plasticity of dendritic excitability. *J Neurobiol* 64:100–115.
- Gasparini S, Losonczy A, Chen X, Johnston D, Magee JC (2007) Associative pairing enhances action potential back-propagation in radial oblique branches of CA1 pyramidal neurons. *J Physiol* 580:787–800.
- Golding NL, Staff NP, Spruston N (2002) Dendritic spikes as a mechanism for cooperative long-term potentiation. *Nature* 418:326–331.
- Haberly L, Behan M (1983) Structure of the piriform cortex of the opossum. III. Ultrastructural characterization of synaptic terminals of association and olfactory bulb afferent fibers. *J Comp Neurol* 219:448–460.
- Harvey CD, Svoboda K (2007) Locally dynamic synaptic learning rules in pyramidal neuron dendrites. *Nature* 450:1195–1200.
- Higley MJ, Sabatini BL (2008) Calcium signaling in dendrites and spines: practical and functional considerations. *Neuron* 59:902–913.
- Hoffman DA, Johnston D (1999) Neuromodulation of dendritic action potentials. *J Neurophysiol* 81:408–411.
- Hoffman DA, Magee JC, Colbert CM, Johnston D (1997) K^+ channel regulation of signal propagation in dendrites of hippocampal pyramidal neurons. *Nature* 387:869–875.
- Jung MW, Larson J, Lynch G (1990a) Role of NMDA and non-NMDA receptors in synaptic transmission in rat piriform cortex. *Exp Brain Res* 82:451–455.
- Jung MW, Larson J, Lynch G (1990b) Long-term potentiation of monosynaptic EPSPs in rat piriform cortex in vitro. *Synapse* 6:279–283.
- Kampa BM, Stuart GJ (2006) Calcium spikes in basal dendrites of layer 5 pyramidal neurons during action potential bursts. *J Neurosci* 26:7424–7432.
- Kampa BM, Clements J, Jonas P, Stuart GJ (2004) Kinetics of Mg^{2+} unblock of NMDA receptors: implications for spike-timing dependent synaptic plasticity. *J Physiol* 556:337–345.
- Kampa BM, Letzkus JJ, Stuart GJ (2006) Requirement of dendritic calcium spikes for induction of spike-timing-dependent synaptic plasticity. *J Physiol* 574:283–290.
- Kampa BM, Letzkus JJ, Stuart GJ (2007) Dendritic mechanisms controlling spike-timing-dependent synaptic plasticity. *Trends Neurosci* 30:456–463.
- Kanter ED, Haberly LB (1990) NMDA-dependent induction of long-term potentiation in afferent and association fiber systems of piriform cortex in vitro. *Brain Res* 525:175–179.
- Kerchner GA, Nicoll RA (2008) Silent synapses and the emergence of a postsynaptic mechanism for LTP. *Nat Rev Neurosci* 9:813–825.
- Kim J, Jung SC, Clemens AM, Petralia RS, Hoffman DA (2007) Regulation of dendritic excitability by activity-dependent trafficking of the A-type K^+ channel subunit Kv4.2 in hippocampal neurons. *Neuron* 54:933–947.
- Koester HJ, Sakmann B (1998) Calcium dynamics in single spines during coincident pre- and postsynaptic activity depend on relative timing of back-propagating action potentials and subthreshold excitatory postsynaptic potentials. *Proc Natl Acad Sci U S A* 95:9596–9601.
- Larkum ME, Kaiser KM, Sakmann B (1999a) Calcium electrogenesis in distal apical dendrites of layer 5 pyramidal cells at a critical frequency of back-propagating action potentials. *Proc Natl Acad Sci U S A* 96:14600–14604.
- Larkum ME, Zhu JJ, Sakmann B (1999b) A new cellular mechanism for coupling inputs arriving at different cortical layers. *Nature* 398:338–341.
- Larkum ME, Waters J, Sakmann B, Helmchen F (2007) Dendritic spikes in apical dendrites of neocortical layer 2/3 pyramidal neurons. *J Neurosci* 27:8999–9008.
- Larkum ME, Watanabe S, Lasser-Ross N, Rhodes P, Ross WN (2008) Dendritic properties of turtle pyramidal neurons. *J Neurophysiol* 99:683–694.
- Letzkus JJ, Kampa BM, Stuart GJ (2006) Learning rules for spike timing-dependent plasticity depend on dendritic synapse location. *J Neurosci* 26:10420–10429.
- Luna VM, Schoppa NE (2008) GABAergic circuits control input-spike coupling in the piriform cortex. *J Neurosci* 28:8851–8859.
- Magee JC, Johnston D (1997) A synaptically controlled, associative signal for Hebbian plasticity in hippocampal neurons. *Science* 275:209–213.
- Markram H, Lübke J, Frotscher M, Sakmann B (1997) Regulation of synaptic efficacy by coincidence of postsynaptic APs and EPSPs. *Science* 275:213–215.
- Matsuzaki M, Honkura N, Ellis-Davies GC, Kasai H (2004) Structural basis of long-term potentiation in single dendritic spines. *Nature* 429:761–766.
- Mokin M, Keifer J (2006) Quantitative analysis of immunofluorescent punctate staining of synaptically localized proteins using confocal microscopy and stereology. *J Neurosci Methods* 157:218–224.
- Nevian T, Sakmann B (2004) Single spine Ca^{2+} signals evoked by coincident EPSPs and backpropagating action potentials in spiny stellate cells of layer 4 in the juvenile rat somatosensory barrel cortex. *J Neurosci* 24:1689–1699.
- Nevian T, Sakmann B (2006) Spine Ca^{2+} signaling in spike-timing-dependent plasticity. *J Neurosci* 26:11001–11013.
- Neville KR, Haberly LB (2004) Olfactory cortex. In: *The synaptic organization of the brain*, Ed 5 (Shepherd GM, ed), pp 415–454. New York: Oxford UP.
- Pérez-Garci E, Gassmann M, Bettler B, Larkum ME (2006) The GABAB1b isoform mediates long-lasting inhibition of dendritic Ca^{2+} spikes in layer 5 somatosensory pyramidal neurons. *Neuron* 50:603–616.
- Pike FG, Meredith RM, Olding AW, Paulsen O (1999) Rapid report: postsynaptic bursting is essential for “Hebbian” induction of associative long-term potentiation at excitatory synapses in rat hippocampus. *J Physiol* 518:571–576.
- Poo C, Isaacson JS (2007) An early critical period for long-term plasticity and structural modification of sensory synapses in olfactory cortex. *J Neurosci* 27:7553–7558.
- Poo C, Isaacson JS (2009) Odor representations in olfactory cortex: “sparse” coding, global inhibition, and oscillations. *Neuron* 62:850–861.
- Saar D, Grossman Y, Barkai E (2001) Long-lasting cholinergic modulation underlies rule learning in rats. *J Neurosci* 21:1385–1392.
- Sabatini BL, Oertner TG, Svoboda K (2002) The life cycle of Ca^{2+} ions in dendritic spines. *Neuron* 33:439–452.

- Shepherd GM (2004) Introduction to synaptic circuits. In: The synaptic organization of the brain, Ed 5 (Shepherd GM, ed), pp 1–39. New York: Oxford UP.
- Sjöström PJ, Häusser M (2006) A cooperative switch determines the sign of synaptic plasticity in distal dendrites of neocortical pyramidal neurons. *Neuron* 51:227–238.
- Sjöström PJ, Rancz EA, Roth A, Häusser M (2008) Dendritic excitability and synaptic plasticity. *Physiol Rev* 88:769–840.
- Suzuki N, Bekkers JM (2006) Neural coding by two classes of principal cells in the mouse piriform cortex. *J Neurosci* 26:11938–11947.
- Tang AC, Hasselmo ME (1994) Selective suppression of intrinsic but not afferent fiber synaptic transmission by baclofen in the piriform (olfactory) cortex. *Brain Res* 659:75–81.
- Waters J, Larkum M, Sakmann B, Helmchen F (2003) Supralinear Ca^{2+} influx into dendritic tufts of layer 2/3 neocortical pyramidal neurons *in vitro* and *in vivo*. *J Neurosci* 23:8558–8567.
- Wilson DA (1998) Habituation of odor responses in the rat anterior piriform cortex. *J Neurophysiol* 79:1425–1440.
- Yuste R, Denk W (1995) Dendritic spines as basic functional units of neuronal integration. *Nature* 375:682–684.